Nonequilibrium Hole Dynamics in Antiferromagnets: Damped Strings and Polarons

K. Knakkergaard Nielsen [1,2] T. Pohl,[2] and G. M. Bruun[2,3]

[1]*Max-Planck Institute for Quantum Optics, Hans-Kopfermann-Strasse 1, D-85748 Garching, Germany*
[2]*Department of Physics and Astronomy, Aarhus University, Ny Munkegade, 8000 Aarhus C, Denmark*
[3]*Shenzhen Institute for Quantum Science and Engineering and Department of Physics,*
Southern University of Science and Technology, Shenzhen 518055, China

We develop a nonperturbative theory for hole dynamics in antiferromagnetic spin lattices, as described by the *t-J* model. This is achieved by generalizing the self-consistent Born approximation to nonequilibrium systems, making it possible to calculate the full time-dependent many-body wave function. Our approach reveals three distinct dynamical regimes, ultimately leading to the formation of magnetic polarons. Following the initial ballistic stage of the hole dynamics, coherent formation of string excitations gives rise to characteristic oscillations in the hole density. Their damping eventually leaves behind magnetic polarons that undergo ballistic motion with a greatly reduced velocity. The developed theory provides a rigorous framework for understanding nonequilibrium physics of defects in quantum magnets and quantitatively explains recent observations from cold-atom quantum simulations in the strong coupling regime.

Understanding the motion of charge carriers in quantum spin environments is of great fundamental significance in condensed matter physics [1–5]. Recently, this problem is attracting growing interest [6–15], driven by the success of quantum simulations with ultracold atoms in optical lattices [16,17]. In particular, the realization of the Fermi-Hubbard model [16,18–33] combined with single-site resolution techniques [34–37] makes it possible to probe the structure and quantum dynamics of lattice defects on a microscopic level [25,26,32]. The behavior of holes in the Fermi-Hubbard model and the associated formation of magnetic polarons is intimately connected to the physics of high-temperature superconductivity [38–40]. Their dynamics, furthermore, constitutes a paradigmatic example of a strongly interacting quantum many-body system out of equilibrium, whose rigorous description has remained an open theoretical problem. Quantum Monte Carlo simulations [6,7] have allowed us to study the short-time dynamics at infinite temperature and discover a crossover from an initial—ballistic—quantum walk toward a diffusive regime. Recent cold-atom experiments traced the microscopic motion of holes in a simulated Fermi-Hubbard model [32] and, instead, found a crossover to another ballistic regime with a reduced effective hole velocity. This experimentally indicates the creation of magnetic polarons and raises exciting open questions about the dynamical process of quasiparticle formation [41] and their emerging transport properties.

Here, we address this problem and develop a rigorous theoretical framework for the nonequilibrium dynamics of holes in an antiferromagnetic spin lattice. Our starting point is the self-consistent Born approximation (SCBA) known to be quantitatively accurate under equilibrium conditions [15,42,43]. We generalize this approach to nonequilibrium situations and derive a recursion relation for the time-dependent many-body wave function of the quantum magnet. This makes it possible to describe the complex quantum dynamics of interacting spins as the hole propagates through the underlying antiferromagnetic lattice, accounting for an arbitrary number of spin excitations. Our theory provides a remarkably accurate description of the experimentally observed hole motion at all measured times and strong interactions [see Fig. 1(b)]. The calculations reveal three dynamical regimes that characterize the dynamical emergence of magnetic polarons from localized lattice defects [Fig. 1(c)]. The theory predicts a ballistic hole expansion with a universal initial velocity that is independent of the interaction strength [red region in Fig. 1(c)]. At intermediate times (blue region), the dynamics is characterized by the formation of magnetic polaron states as well as string excitations, in which the hole is confined in the linear potential of flipped spins in its trail [1,9,44,45]. Quantum interference between the polarons and the string excitations leads to characteristic oscillations in the hole dynamics consistent with experimental observations [32]. Ultimately, string excitations are found to dampen at long times, with emergent quasiparticle behavior and ballistic propagation of polarons with a reduced velocity [green region in Fig. 1(c)].

The system.—We consider the motion of a single hole in a two-component (spin $\sigma = \uparrow, \downarrow$) Fermi gas in a 2D square lattice. For strong repulsion, the two spins form a quantum
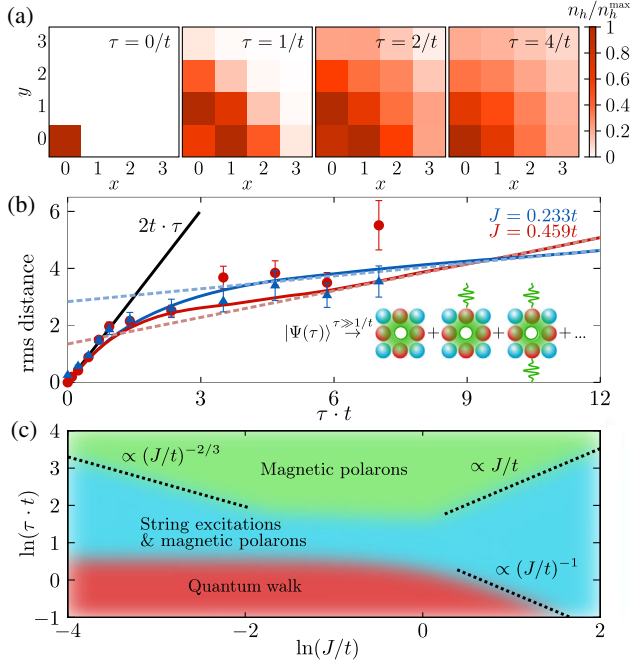
FIG. 1. Nonequilibrium hole dynamics. (a) The hole density $n_h(\mathbf{d})$ for $J = 0.233t$ and different times normalized to its maximal value $n_h^{\max}$ is shown in the first quadrant of the lattice, exploiting the C_4 rotational symmetry. (b) Root-mean-square distance of the hole as a function of time for indicated interaction strengths compared to experimental results. At long times, the dynamics is determined by ballistic propagation of magnetic polarons (white hole surrounded by red $\sigma = \uparrow$ and blue $\sigma = \downarrow$ fermions), dressed by spin waves (green waves) (inset). (c) We find three distinct dynamical regimes: a quantum walk at short times (red), interfering string excitations at intermediate times (blue), and ballistic transport of magnetic polarons at long times (green).

antiferromagnet and the system can be described by the t-J model [40,46]. Using a slave-fermion representation, this problem can be mapped to the Hamiltonian

$$\hat{H} = \sum_{\mathbf{k}} \omega_{\mathbf{k}} \hat{b}_{\mathbf{k}}^\dagger \hat{b}_{\mathbf{k}} + \sum_{\mathbf{q},\mathbf{k}} g(\mathbf{q},\mathbf{k})[\hat{h}_{\mathbf{q}+\mathbf{k}}^\dagger \hat{h}_{\mathbf{q}} \hat{b}_{-\mathbf{k}}^\dagger + \text{H.c.}] \quad (1)$$

within linear spin wave theory [2,4]. Here, $\hat{b}_{\mathbf{k}}^\dagger$ is a bosonic operator creating a spin wave with crystal momentum $\mathbf{k}$ and energy $\omega_{\mathbf{k}} = 2J\sqrt{1 - \gamma_{\mathbf{k}}^2}$, where $J > 0$ is the antiferromagnetic coupling between neighboring spins and $\gamma_{\mathbf{k}} = [\cos(k_x) + \cos(k_y)]/2$ is a structure factor, taking the lattice constant to be unity. The second term in Eq. (1) describes how the motion of holes created by the fermionic operator $\hat{h}_{\mathbf{k}}$ makes spin excitations above the antiferromagnetic (AFM) ground state defined by $\hat{b}_{\mathbf{k}}|\text{AFM}\rangle = 0$. The associated vertex strength is $g(\mathbf{q},\mathbf{k}) = 4t \cdot (u_{\mathbf{k}} \gamma_{\mathbf{q}+\mathbf{k}} - v_{\mathbf{k}} \gamma_{\mathbf{q}})/\sqrt{N}$ with N the number of lattice

sites, t the hopping strength, and $u_{\mathbf{k}} = [(1/\sqrt{1 - \gamma_{\mathbf{k}}^2} + 1)/2]^{1/2}$ and $v_{\mathbf{k}} = \text{sgn}(\gamma_{\mathbf{k}})[(1/\sqrt{1 - \gamma_{\mathbf{k}}^2} - 1)/2]^{1/2}$ the coherence factors. The t-J model is an effective low-energy description for strong coupling, $J \ll t$, of the Hubbard model realized experimentally [40,46]; we therefore predominantly focus on this regime.

Time-dependent SCBA.—We now describe our time-dependent theory for hole dynamics in the antiferromagnetic lattice. To describe the experimental situation, we initiate a single hole at the site $\mathbf{d} = \mathbf{0}$, i.e., $|\Psi(\tau = 0)\rangle = \hat{h}_{\mathbf{0}}^\dagger|\text{AFM}\rangle = \sum_{\mathbf{p}} \hat{h}_{\mathbf{p}}^\dagger|\text{AFM}\rangle/\sqrt{N}$, with τ the variable of time to distinguish it from the hopping t. We then have $|\Psi(\tau)\rangle = \sum_{\mathbf{p}} |\Psi_{\mathbf{p}}(\tau)\rangle/\sqrt{N}$, with $i\partial_\tau|\Psi_{\mathbf{p}}(\tau)\rangle = \hat{H}|\Psi_{\mathbf{p}}(\tau)\rangle$. We write $|\Psi_{\mathbf{p}}(\tau)\rangle = |\Psi_{\mathbf{p}}^R(\tau)\rangle + |\Psi_{\mathbf{p}}^A(\tau)\rangle$, where $|\Psi_{\mathbf{p}}^R(\tau)\rangle = \exp(-\eta\tau)\theta(\tau) \cdot |\Psi_{\mathbf{p}}(\tau)\rangle$ and $|\Psi_{\mathbf{p}}^A(\tau)\rangle = \exp(\eta\tau)\theta(-\tau) \cdot |\Psi_{\mathbf{p}}(\tau)\rangle$ are the retarded and advanced wave functions. Fourier transforming the Schrödinger equation then yields (see Supplemental Material [47])

$$(\omega + i\eta)|\Psi_{\mathbf{p}}^R(\omega)\rangle = i|\Psi_{\mathbf{p}}(\tau = 0)\rangle + \hat{H}|\Psi_{\mathbf{p}}^R(\omega)\rangle. \quad (2)$$

The advanced state is found by $|\Psi_{\mathbf{p}}^A(\omega)\rangle = [|\Psi_{\mathbf{p}}^R(\omega)\rangle]^*$. In principle, $|\Psi_{\mathbf{p}}^R(\omega)\rangle$ may be expanded in the number of spin waves. For strong coupling, $J/t \ll 1$, however, the corresponding expansion does not truncate in a controlled way and requires the inclusion of spin waves to *infinite* order.

We resolve this problem by generalizing the SCBA [2,4] to nonequilibrium conditions. Note that this approximation yields quantitatively accurate results for the hole Green's function compared to exact diagonalization on small systems [42] and Monte Carlo simulations [15]. In the spirit of the SCBA, we retain only noncrossing terms in the equations of motion for the expansion coefficients of the wave function to obtain a recursion relation for the retarded wave function [47]

$$|\Psi_{\mathbf{p}}^R(\omega)\rangle = G^R(\mathbf{p}, \omega)[i\hat{h}_{\mathbf{p}}^\dagger|\text{AFM}\rangle$$
$$+ \sum_{\mathbf{k}} g(\mathbf{p}, \mathbf{k}) \cdot \hat{b}_{-\mathbf{k}}^\dagger|\Psi_{\mathbf{p}+\mathbf{k}}^R(\omega - \omega_{\mathbf{k}})\rangle]. \quad (3)$$

Here, $G^R(\mathbf{p}, \omega) = [\omega - \Sigma(\mathbf{p}, \omega) + i\eta]^{-1}$ is the retarded hole Green's function with the SCBA self-energy $\Sigma(\mathbf{p}, \omega) = \sum_{\mathbf{k}} g^2(\mathbf{p}, \mathbf{k})G^R(\mathbf{p} + \mathbf{k}, \omega - \omega_{\mathbf{k}})$ [2,4]. The recursive structure in Eq. (3) is similar to the SCBA magnetic polaron states [14,49] and allows us to compute the nonequilibrium hole dynamics in an efficient and accurate manner taking an infinite number of spin waves into account. This yields a rigorous generalization of the SCBA to the time-dependent case and represents the main result of this Letter.

Using the single-site resolution of quantum gas microscopes, one can measure the hole density $n_h(\mathbf{d}, \tau) = \langle\Psi(\tau)|\hat{h}_{\mathbf{d}}^\dagger \hat{h}_{\mathbf{d}}|\Psi(\tau)\rangle$ at a given position $\mathbf{d}$ and time τ [32]. Here, we obtain it from

$$n_h(\mathbf{d}, \tau) = \frac{1}{N} \sum_{\mathbf{q}} e^{-i\mathbf{q}\cdot\mathbf{d}} \int \frac{d\nu}{2\pi} N_h(\mathbf{q}, \nu), \qquad (4)$$

where $N_h(\mathbf{q}, \nu) = (2\pi)^{-1} \sum_{\mathbf{p}} \int d\omega N_h(\mathbf{q}, \nu; \mathbf{p}, \omega)$ and $N_h(\mathbf{q}, \nu; \mathbf{p}, \omega) = \sum_{\mathbf{k}} \langle \Psi_{\mathbf{p}+\mathbf{q}}(\omega + \nu) | \hat{h}_{\mathbf{p}+\mathbf{q}+\mathbf{k}}^{\dagger} \hat{h}_{\mathbf{p}+\mathbf{k}} | \Psi_{\mathbf{p}}(\omega) \rangle$. Using Eq. (3), we derive self-consistency equations for N_h (see Supplemental Material [47]), whereby the time-dependent hole density $n_h(\mathbf{d}, \tau)$ is determined nonperturbatively. We note that the SCBA is a preserving approximation, whereby the total density of holes remains unity, $\sum_{\mathbf{d}} n_h(\mathbf{d}, \tau) = 1$.

Hole dynamics.—In Fig. 1(a), we plot the hole density in the lattice at different times for $J = 0.233t$. This illustrates the spatial expansion of the hole following its localized creation at site $\mathbf{d} = \mathbf{0}$. From the density, we determine the rms distance $d_{\mathrm{rms}}(\tau) = [\sum_{\mathbf{d}} d^2 \cdot n_h(\mathbf{d}, \tau)]^{1/2}$, which is compared to experimental measurements [32] in Fig. 1(b) for two different coupling strengths. We find a clear crossover between distinct regimes of ballistic expansion with $d = v\tau$ with different velocities v. The final expansion velocity is greatly reduced compared to a quantum walk of the hole. For the relevant case of strong coupling, $J = 0.233t$, for which the t-J model accurately describes the underlying Fermi-Hubbard Hamiltonian, our theory agrees quantitatively with the experimental data across all timescales. For $J = 0.459t$, the agreement is expectedly not as good, since the mapping from the Fermi-Hubbard Hamiltonian, realized in the experiment [32], to the t-J model becomes less accurate as J/t increases [40].

The expansion dynamics is investigated in more detail in Fig. 2, which displays the rms distance and the associated expansion velocity $v_{\mathrm{rms}} = \partial_\tau d_{\mathrm{rms}}$ for a range of interaction strengths. This shows that the crossover to the long-time ballistic motion of the polaron slows down with increasing
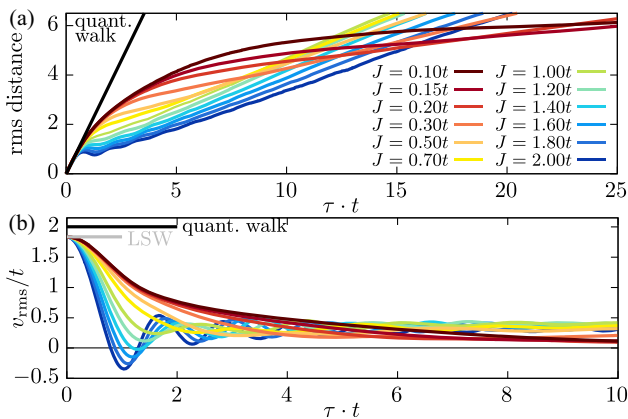

(a)
(b)

FIG. 2. rms distance distance and velocity (a) Time evolution of the rms distance d_{rms} for different indicated values of J/t. (b) The rms velocity $v_{\mathrm{rms}} = \partial_\tau d_{\mathrm{rms}}$ for the same interaction strengths. The black line corresponds to a free quantum walk with $v_{\mathrm{rms}}^0 = 2t$, while the gray line, $v_{\mathrm{rms}}^0 \simeq 1.84t$, follows from linear spin wave theory.

interaction strength t/J. Physically, a hole in a lattice with a smaller spin-spin coupling J will move further away from its initial position before it is affected by the underlying spin order of the quantum magnet. However, a smaller J also implies stronger dressing of the hole by spin waves in its final polaron state. This slows down the long-time ballistic expansion and thereby leads to the nontrivial crossing of the lines in Fig. 2(a). The calculated dynamics reveals three distinct dynamical regimes: (i) an initial quantum walk of the hole, (ii) a crossover stage driven by string excitations, and (iii) the final formation of magnetic polarons.

(i) *Quantum walk.* The results of Figs. 1 and 2 indicate universal initial hole dynamics that follows a ballistic expansion with a J-independent velocity, v_{rms}^0. Indeed, the short-time expansion of the t-J model yields a free quantum walk to leading order in τ with a ballistic expansion velocity $v_{\mathrm{rms}}^0 = 2t$ [47,50], also observed experimentally [32]. The linear spin wave approximation yields a slightly lower velocity of $v_{\mathrm{rms}}^0 = 1.84t$ differing from the exact result by only ~8% [Fig. 2(b)]. Expanding our wave function at short times gives $d_{\mathrm{rms}} \simeq v_{\mathrm{rms}}^0 \cdot \tau[1 - c_3 \cdot (t \cdot \tau)^2]$, where $c_3 = c_3^{(0)} + c_3^{(J)} \cdot (J/t)^2$, with interaction-independent coefficients $c_3^{(0)}$ and $c_3^{(J)}$ [47]. Setting $1 - c_3(t\tau_s)^2 = 1/2$ allows us to define the timescale

$$\tau_s = \frac{1}{t\sqrt{2[c_3^{(0)} + c_3^{(J)} \cdot (J/t)^2]}}, \qquad (5)$$

after which the initial ballistic behavior breaks down, defining the initial regime shown by the red area in Fig. 1(c). Consequently, we find τ_s is proportional to $1/t$ and $1/J$ for strong $J \ll t$ and weak coupling $J \gg t$, respectively.

(ii) *Interfering string excitations.* After the initial universal ballistic expansion, the dynamics enters a second regime characterized by oscillations of the hole velocity with a period that increases with the interaction strength t/J. This is explored further in Fig. 3, where we show the density of holes around its initial position $\mathbf{d} = \mathbf{0}$, revealing significant oscillations consistent with the experimental observations [32]. The agreement between theory and experiment is particularly good at $d = 0$ and $d = 1$ [Figs. 3(a) and 3(b)], while accurate comparisons at larger distances are hindered by a decreasing signal-to-noise ratio [32]. To understand the origin of these oscillations, we show the total density of states (DOS) $A(\omega) = \sum_{\mathbf{p}} A(\mathbf{p}, \omega)/N$ for $J/t = 0.233$ in Fig. 3(e) and as a function of J/t in Fig. 3(f). Here, $A(\mathbf{p}, \omega)$ is the hole spectral function (see Supplemental Material [47]). One clearly observes multiple peaks in the DOS, the lowest corresponding to the emerging magnetic polaron. Figure 3(f) also shows a characteristic $(J/t)^{2/3}$ scaling of the position of the high-frequency peaks. This is consistent with string excitations, which correspond to Airy-like
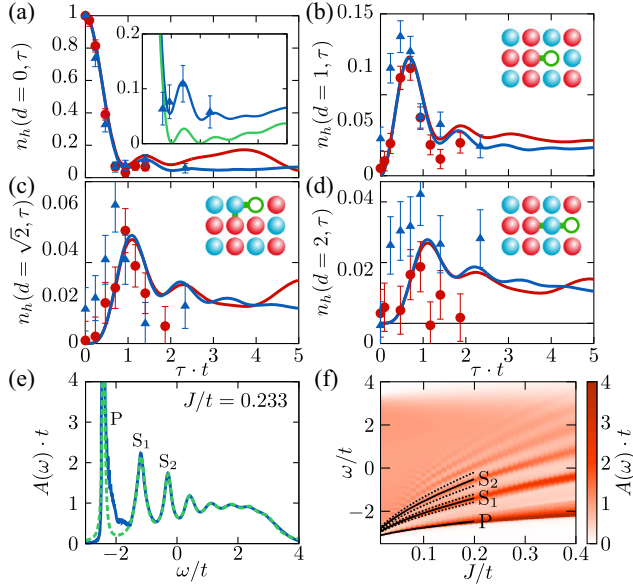
FIG. 3.   Local hole density and string excitations. (a)–(d) The hole density as a function of time for $J = 0.459t$ (red) and $J = 0.233t$ (blue) for different indicated distances d. The experimental data are shown by red dots for $J = 0.459t$ and by blue triangles for $J = 0.233t$. (e) Total density of states $A(\omega)$ with a multi-Lorentzian fit (dashed green line). In the inset of (a), the norm square of the Fourier transform of this fit (green line) is compared to the full solution and experimental data (blue) for $J = 0.233t$. The low-frequency peak of $A(\omega)$ corresponds to magnetic polarons (P). The higher-lying peaks reflect string excitations (S_i). Their energies and spectral widths exhibit a characteristic $(J/t)^{2/3}$ scaling for $J/t \ll 1$, shown by black lines in (f).

eigenstates of the hole, confined in the linear potential formed by its trail of flipped spins. In the strong coupling limit of the $t - J_z$ model, this effective potential has a strength $\propto J_z$ [4,44]. The presence of transverse spin-spin couplings broadens the string excitations [15,45], and using a multi-Lorentzian fit [Fig. 3(e)] we find that their spectral widths show the same $(J/t)^{2/3}$ scaling as their energies.

To see how these excitations contribute to the intermediate hole dynamics, we compute the Fourier transform of the Lorentzian fit $G(\tau)$, which exclusively captures the contribution from the different peaks. Its norm square $|G(\tau)|^2$ recovers the oscillatory hole motion as shown in the inset of Fig. 3(a). Indeed, it follows from Eq. (3) that $|G(\tau)|^2$ determines the hole density at the initial site $\mathbf{d} = \mathbf{0}$ to lowest order. We conclude from Fig. 3(a) that the oscillations arise due to quantum interference between the polaron states and the string excitations. In the strongly interacting regime, $J \ll t$, these oscillations stretch out as the spacing between the associated energies diminishes [Fig. 3(f)]. This interference process defines the second dynamical regime [blue region in Fig. 1(c)], while the lifetime of the lowest string excitation [marked as S_1 in Fig. 3(f)] determines the dynamical crossover into the final propagation stage. The corresponding transition time scales as $(J/t)^{-2/3}$ and J/t for strong and weak coupling, respectively, and is shown by the upper lines in Fig. 1(c).

(iii) Magnetic polarons. Following the damping of string excitations, the remaining superposition of magnetic polaron states once more undergoes ballistic expansion, at a greatly reduced velocity, evident both from Figs. 1(b) and 2. Indeed, at times longer than the string lifetime, we can write our wave function as [47]

$$|\Psi(\tau)\rangle \rightarrow \frac{1}{\sqrt{N}} \sum_{\mathbf{p}} \left[\sqrt{Z_{\mathbf{p}}} e^{-i\varepsilon_{\mathbf{p}}\tau} |\Psi_{\mathbf{p}}^{\text{pol}}\rangle + \sum_{\mathbf{k}} g_1(\mathbf{p},\mathbf{k}) \sqrt{Z_{\mathbf{p}+\mathbf{k}}} e^{-i(\varepsilon_{\mathbf{p}+\mathbf{k}}+\omega_{\mathbf{k}})\tau} \hat{b}_{-\mathbf{k}}^{\dagger} |\Psi_{\mathbf{p}+\mathbf{k}}^{\text{pol}}\rangle + \cdots \right], \qquad (6)$$

where $g_1(\mathbf{p},\mathbf{k}) = g(\mathbf{p},\mathbf{k})\text{Re}[G^R(\mathbf{p},\varepsilon_{\mathbf{p}+\mathbf{k}} + \omega_{\mathbf{k}})]$. The first term in Eq. (6) corresponds to the ballistic propagation of magnetic polarons $|\Psi_{\mathbf{p}}^{\text{pol}}\rangle$ with crystal momentum $\mathbf{p}$, energy $\varepsilon_{\mathbf{p}}$, and quasiparticle residue $Z_{\mathbf{p}}$. The second term describes polaron propagation along with a spin wave and is the first term in a series in the number of spin waves [Fig. 1(b), inset]. These asymptotics explicitly confirm the dynamical formation of magnetic polarons, indicated by experiments [32].

In Fig. 4(a), we show the asymptotic expansion velocity v_{rms}^{∞}. Motivated by the propagation of magnetic polarons evident from Eq. (6), we also plot the average polaron group velocity $v_{\text{rms}}^{\text{pol}} = [\sum_{\mathbf{p}} (\nabla_{\mathbf{p}} \varepsilon_{\mathbf{p}})^2 / N]^{1/2}$. In the perturbative limit, the first term in Eq. (6) dominates, and v_{rms}^{∞} and

$v_{\text{rms}}^{\text{pol}}$ both approach an asymptotic value of $0.41 w_{\text{pol}}$ [47], evident in Fig. 4(a) for $J/t \gtrsim 1$. Below $J/t \simeq 0.4$, however, these two velocities start to deviate significantly. This originates in a qualitative change in the quasiparticle residues, which become very small in certain regions of the Brillouin zone for strong interactions (see Supplemental Material [47]). As a result, the associated polaron states do not contribute to the long-time dynamics, leading to a sublinear dependency of the expansion velocity on J [Fig. 4(a)], even though the polaron bandwidth approaches $w_{\text{pol}} \sim 2J$ [4,51]. For very strong coupling $J/t \lesssim 0.02$ [52], it is expected that the ground state of the system develops a growing region of ferromagnetic correlations, the so-called Nagaoka limit [53]. While we
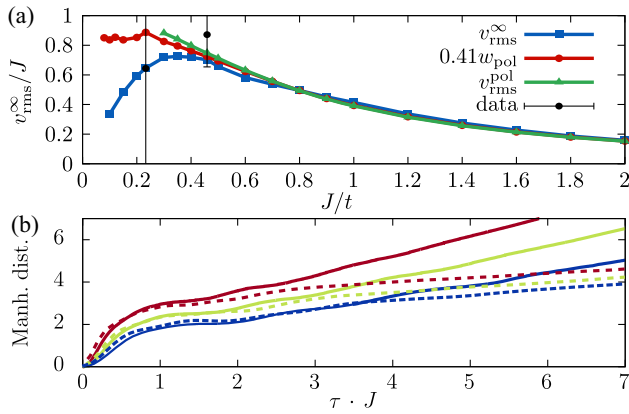
FIG. 4. Expansion velocity and comparison with MPS simulations. (a) Long-time expansion velocity v_{rms}^{∞} (blue squares), rescaled polaron bandwidth $w_{pol} = \min_{\mathbf{p}} \varepsilon_{\mathbf{p}} - \max_{\mathbf{p}} \varepsilon_{\mathbf{p}}$ (red dots), and average polaronic group velocity v_{rms}^{pol} (green triangles) in units of J as a function of J/t. The experimentally observed velocities are shown by the black dots. (b) Manhattan distance for $J/t = 0.35$ (red), 0.5 (green), and 0.7 (blue) obtained from our dynamical SCBA theory (solid lines) compared to the results of numerical MPS simulations (dashed lines) [41].

observe indications of this behavior [14], the total spin is conserved under the dynamical evolution, which makes it difficult to observe large ferromagnetic domains in the limit of very small values of J/t. The importance of this effect for the motion of holes, hence remains an interesting topic for future investigations.

In Fig. 4(b), we compare our results for the Manhattan distance $\sum_{\mathbf{d}} (|d_x| + |d_y|) \cdot n_h(\mathbf{d}, \tau)$ to recent numerical simulations of the t-J model using matrix product states (MPSs) [41]. The good agreement with the numerical results found at short times confirms the accuracy of our approach. At longer times, however, we observe significant deviations, which must be expected due to finite size effects when the Manhattan distance exceeds half the circumference of the 4×18 cylindrical lattice simulated in Ref. [41]. Reaching large system sizes remains a challenge in numerical simulations, such that the presented theory offers an important approach to explore the dynamics of lattice defects and quasiparticle formation over the complete range of relevant timescales.

Conclusions.—We have developed a nonperturbative approach for computing the nonequilibrium dynamics of holes in Heisenberg antiferromagnets. Our theory provides a quantitative explanation of recent results from cold-atom experiments [32] at strong interactions. The method yields a complete characterization of the quantum motion of holes and reveals three distinct dynamical regimes that characterize the emergence and evolution of magnetic polarons. It explains observed oscillatory behavior in terms of quantum interference between polarons and string excitations. The presented formalism offers a powerful framework to describe the nonequilibrium quantum dynamics of

impurities in strongly interacting lattice models. For example, the method could be utilized to analyze spectroscopic measurements [54] of holes. Cold-atom experiments also make it possible to probe spin correlations induced by adjacent holes [25,26]. Our approach can be used to describe the dynamical buildup of such correlations and may reveal the dynamics of correlations between two holes, which could provide new insights into pairing and potential mechanisms for high-temperature superconductivity at low doping [39,46,55–58]. Finally, understanding the impact of temperature on the properties of magnetic polarons [59] remains a challenging open problem, which we hope to explore in the future.

[1] W. F. Brinkman and T. M. Rice, Phys. Rev. B **2**, 1324 (1970).
[2] S. Schmitt-Rink, C. M. Varma, and A. E. Ruckenstein, Phys. Rev. Lett. **60**, 2793 (1988).
[3] B. I. Shraiman and E. D. Siggia, Phys. Rev. Lett. **61**, 467 (1988).
[4] C. L. Kane, P. A. Lee, and N. Read, Phys. Rev. B **39**, 6880 (1989).
[5] S. A. Trugman, Phys. Rev. B **41**, 892 (1990).
[6] J. Carlström, N. Prokof'ev, and B. Svistunov, Phys. Rev. Lett. **116**, 247202 (2016).
[7] M. Kanász-Nagy, I. Lovas, F. Grusdt, D. Greif, M. Greiner, and E. A. Demler, Phys. Rev. B **96**, 014303 (2017).
[8] F. Grusdt, Z. Zhu, T. Shi, and E. Demler, SciPost Phys. **5**, 57 (2018).
[9] F. Grusdt, M. Kánasz-Nagy, A. Bohrdt, C. S. Chiu, G. Ji, M. Greiner, D. Greif, and E. Demler, Phys. Rev. X **8**, 011046 (2018).
[10] F. Grusdt, A. Bohrdt, and E. Demler, Phys. Rev. B **99**, 224422 (2019).
[11] A. Bohrdt, C. S. Chiu, G. Ji, M. Xu, D. Greif, M. Greiner, E. Demler, F. Grusdt, and M. Knap, Nat. Phys. **15**, 921 (2019).
[12] A. Bohrdt, Y. Wang, J. Koepsell, M. Kánasz-Nagy, E. Demler, and F. Grusdt, Phys. Rev. Lett. **126**, 026401 (2021).
[13] D. Soriano and M. I. Katsnelson, Phys. Rev. B **101**, 041402 (R) (2020).
[14] K. K. Nielsen, M. A. Bastarrachea-Magnani, T. Pohl, and G. M. Bruun, Phys. Rev. B **104**, 155136 (2021).
[15] N. Diamantis and E. Manousakis, New J. Phys. **23**, 123005 (2021).
[16] T. Esslinger, Annu. Rev. Condens. Matter Phys. **1**, 129 (2010).

[17] C. Gross and I. Bloch, Science **357**, 995 (2017).
[18] M. Boll, T. A. Hilker, G. Salomon, A. Omran, J. Nespolo, L. Pollet, I. Bloch, and C. Gross, Science **353**, 1257 (2016).
[19] L. W. Cheuk, M. A. Nichols, K. R. Lawrence, M. Okan, H. Zhang, E. Khatami, N. Trivedi, T. Paiva, M. Rigol, and M. W. Zwierlein, Science **353**, 1260 (2016).
[20] A. Mazurenko, C. S. Chiu, G. Ji, M. F. Parsons, M. Kanász-Nagy, R. Schmidt, F. Grusdt, E. Demler, D. Greif, and M. Greiner, Nature (London) **545**, 462 (2017).
[21] T. A. Hilker, G. Salomon, F. Grusdt, A. Omran, M. Boll, E. Demler, I. Bloch, and C. Gross, Science **357**, 484 (2017).
[22] P. T. Brown, D. Mitra, E. Guardado-Sanchez, P. Schauß, S. S. Kondov, E. Khatami, T. Paiva, N. Trivedi, D. A. Huse, and W. S. Bakr, Science **357**, 1385 (2017).
[23] C. S. Chiu, G. Ji, A. Mazurenko, D. Greif, and M. Greiner, Phys. Rev. Lett. **120**, 243201 (2018).
[24] P. T. Brown, D. Mitra, E. Guardado-Sanchez, R. Nourafkan, A. Reymbaut, C.-D. Hébert, S. Bergeron, A.-M. S. Tremblay, J. Kokalj, D. A. Huse, P. Schauß, and W. S. Bakr, Science **363**, 379 (2019).
[25] J. Koepsell, J. Vijayan, P. Sompet, F. Grusdt, T. A. Hilker, E. Demler, G. Salomon, I. Bloch, and C. Gross, Nature (London) **572**, 358 (2019).
[26] C. S. Chiu, G. Ji, A. Bohrdt, M. Xu, M. Knap, E. Demler, F. Grusdt, M. Greiner, and D. Greif, Science **365**, 251 (2019).
[27] P. T. Brown, E. Guardado-Sanchez, B. M. Spar, E. W. Huang, T. P. Devereaux, and W. S. Bakr, Nat. Phys. **16**, 26 (2020).
[28] J. Vijayan, P. Sompet, G. Salomon, J. Koepsell, S. Hirthe, A. Bohrdt, F. Grusdt, I. Bloch, and C. Gross, Science **367**, 186 (2020).
[29] T. Hartke, B. Oreg, N. Jia, and M. Zwierlein, Phys. Rev. Lett. **125**, 113601 (2020).
[30] E. Guardado-Sanchez, A. Morningstar, B. M. Spar, P. T. Brown, D. A. Huse, and W. S. Bakr, Phys. Rev. X **10**, 011042 (2020).
[31] J. Koepsell, D. Bourgund, P. Sompet, S. Hirthe, A. Bohrdt, Y. Wang, F. Grusdt, E. Demler, G. Salomon, C. Gross, and I. Bloch, Science **374**, 82 (2021).
[32] G. Ji, M. Xu, L. H. Kendrick, C. S. Chiu, J. C. Brüggenjürgen, D. Greif, A. Bohrdt, F. Grusdt, E. Demler, M. Lebrat, and M. Greiner, Phys. Rev. X **11**, 021022 (2021).
[33] M. Gall, N. Wurz, J. Samland, C. F. Chan, and M. Köhl, Nature (London) **589**, 40 (2021).

[34] W. S. Bakr, J. I. Gillen, A. Peng, S. Fölling, and M. Greiner, Nature (London) **462**, 74 (2009).
[35] J. F. Sherson, C. Weitenberg, M. Endres, M. Cheneau, I. Bloch, and S. Kuhr, Nature (London) **467**, 68 (2010).
[36] E. Haller, J. Hudson, A. Kelly, D. A. Cotta, B. Peaudecerf, G. D. Bruce, and S. Kuhr, Nat. Phys. **11**, 738 (2015).
[37] J. Yang, L. Liu, J. Mongkolkiattichai, and P. Schauss, PRX Quantum **2**, 020344 (2021).
[38] V. J. Emery, Phys. Rev. Lett. **58**, 2794 (1987).
[39] J. R. Schrieffer, X.-G. Wen, and S.-C. Zhang, Phys. Rev. Lett. **60**, 944 (1988).
[40] E. Dagotto, Rev. Mod. Phys. **66**, 763 (1994).
[41] A. Bohrdt, F. Grusdt, and M. Knap, New J. Phys. **22**, 123023 (2020).
[42] G. Martinez and P. Horsch, Phys. Rev. B **44**, 317 (1991).
[43] Z. Liu and E. Manousakis, Phys. Rev. B **44**, 2414 (1991).
[44] L. Bulaevskii, E. Nagaev, and D. Khomskii, J. Exp. Theor. Phys. **27**, 836 (1968).
[45] Z. Liu and E. Manousakis, Phys. Rev. B **45**, 2425 (1992).
[46] Y. A. Izyumov, Phys. Usp. **40**, 445 (1997).
[47] See Supplemental Material at http://link.aps.org/supplemental/10.1103/PhysRevLett.129.246601 for details on the derivation of the nonequilibrium wave function, self-consistency equations, short- and long-time dynamics, and determination of the energy and lifetime of the lowest string excitation, which includes Ref. [49].
[48] A. Ramšak and P. Horsch, Phys. Rev. B **57**, 4308 (1998).
[49] G. F. Reiter, Phys. Rev. B **49**, 1536 (1994).
[50] A. Bohrdt and F. Grusdt (private communication).
[51] E. Dagotto, R. Joynt, A. Moreo, S. Bacci, and E. Gagliano, Phys. Rev. B **41**, 9049 (1990).
[52] S. R. White and I. Affleck, Phys. Rev. B **64**, 024411 (2001).
[53] Y. Nagaoka, Phys. Rev. **147**, 392 (1966).
[54] A. Bohrdt, D. Greif, E. Demler, M. Knap, and F. Grusdt, Phys. Rev. B **97**, 125117 (2018).
[55] B. I. Shraiman and E. D. Siggia, Phys. Rev. B **40**, 9162 (1989).
[56] D. M. Frenkel and W. Hanke, Phys. Rev. B **42**, 6711 (1990).
[57] R. Eder, Phys. Rev. B **45**, 319 (1992).
[58] J. Riera and E. Dagotto, Phys. Rev. B **57**, 8609 (1998).
[59] J.-i. Igarashi and P. Fulde, Phys. Rev. B **48**, 998 (1993).